Plasmon-coupled resonance energy transfer: a real-time electrodynamics approach

Wendu Ding,[1] Liang-Yan Hsu,[1, a)] and George C. Schatz[1, b)]
Department of Chemistry, Northwestern University, 2145 Sheridan Road, Evanston, Illinois 60208-3113, United States

This paper presents a new real-time electrodynamics approach for determining the rate of resonance energy transfer (RET) between two molecules in the presence of plasmonic or other nanostructures (inhomogeneous absorbing and dispersive media). In this approach to plasmon-coupled resonance energy transfer (PC-RET), we develop a classical electrodynamics expression for the energy transfer matrix element which is evaluated using the finite-difference time-domain (FDTD) method to solve Maxwell's equations for the electric field generated by the molecular donor and evaluated at the position of the molecular acceptor. We demonstrate that this approach yields RET rates in homogeneous media that are in precise agreement with analytical theory based on quantum electrodynamics. In the presence of gold nanoparticles, our theory shows that the long-range decay of the RET rates can be significantly modified by plasmon excitation, with rates increased by as much as a factor of 10^6 leading to energy transfer rates over hundreds of nm that are comparable to that over 10s of nm in the absence of the nanoparticles. These promising results suggest important future applications of the PC-RET in areas involving light harvesting or sensing, where energy transfer processes involving inhomogeneous absorbing and dispersive media are commonplace.

Keywords: Plasmonic enhancement, Resonance energy transfer, Classical electrodynamics, FDTD, Time-domain.

I. INTRODUCTION

In recent years, the synthesis of metal nanoparticles has been developed to provide new capabilities for making metal structures with complex tunable geometries and sizes.[1–11] This has enabled significant variation in the physical properties of the nanoparticles,[12–14] and as a result there have been extensive experimental and theoretical studies of plasmonic effects.[3,14–19] Of particular interest is the electromagnetic field at the surface of the particles when localized surface plasmon resonances (LSPR) are excited, as this enables surface enhanced Raman spectroscopy (SERS),[20] plasmonic therapies,[21] chemical and biological sensing,[22–25] and catalysis.[26]

One promising direction of this research involves the use of plasmonic nanostructures to modify the rate of resonance energy transfer (RET) between molecules. RET has been studied for more than half a century, and usually the short-range energy transfer from an excited donor molecule to an acceptor molecule is understood in terms of Förster resonance energy transfer (FRET).[27,28] FRET is a crucial step in the functioning of photovoltaics,[29] photosynthesis,[30–32] biosensing,[33,34] amonst other light harvesting and sensing applications. It is also widely used for nano-scale distance measurement,[35–37] leading to studies of the dynamics of molecular conformations such as protein folding.[38–40] Recently, plasmonic enhancement has been experimentally observed in fluorescence and energy transfer in molecular systems in the vicinity of nanoparticles,[41–46] or between the nanoparticles themselves.[47,48] This motivates the need for a theoretical method for such processes, especially to describe plasmon-coupled resonance energy transfer (PC-RET) under conditions where the donor/acceptor interaction between molecules takes place at long distances in a complex dielectric environment.

As is well known, Förster theory[49–51] leads to an inverse sixth-power distance dependence for RET between molecules in homogeneous media within the electrostatic approximation. It cannot describe long-range effects in RET or molecules in inhomogeneous media. On the other hand, quantum electrodynamics (QED) does properly take long-range effects into account. Based on Fermi's golden rule, the rate of RET can be expressed in terms of the transition matrix element $M(\omega, \mathbf{r_D}, \mathbf{r_A})$ as

$$k_{D\to A}(\omega) = \frac{2\pi}{\hbar}\left|M(\omega, \mathbf{r_D}, \mathbf{r_A})\right|^2 \rho(\omega), \tag{1}$$

where ω is the frequency of the transferred energy (essentially the excitation energy of the acceptor), $\mathbf{r_D}(\mathbf{r_A})$ is the spatial position of the donor (acceptor) particle, and $\rho(\omega)$ is the density of final states associated with energy ω (corresponding to the excited state of the acceptor and the ground state of the donor). In this case, the coupling between donor and acceptor is described by a transition matrix element $M(\omega, \mathbf{r_D}, \mathbf{r_A})$ of the form:[51–58]

$$\begin{aligned} M(\omega, \mathbf{r_D}, \mathbf{r_A}) &= \boldsymbol{\mu}^{\boldsymbol{ge}}(\mathbf{r_D}) \cdot \overset{\leftrightarrow}{\theta}(\omega, \mathbf{r_D}, \mathbf{r_A}) \cdot \boldsymbol{\mu}^{\boldsymbol{eg}}(\mathbf{r_A}) \\ &= \sum_{i,j\in\{1,2,3\}} \mu_i^{ge}(\mathbf{r_D})\theta_{ij}(\omega, \mathbf{r_D}, \mathbf{r_A})\mu_j^{eg}(\mathbf{r_A}), \end{aligned} \tag{2}$$

where the bold symbol $\boldsymbol{\mu}^{\boldsymbol{ge}}(\mathbf{r_D})$ $(\boldsymbol{\mu}^{\boldsymbol{eg}}(\mathbf{r_A}))$ stands for the transition dipole of the donor (acceptor) molecule at the

---

[a)] Electronic mail: liang-yan.hsu@northwestern.edu
[b)] Electronic mail: g-schatz@northwestern.edu

position $\mathbf{r_D}$ ($\mathbf{r_A}$), and $\mu_i^{ge}(\mathbf{r_D})$ is the i-th component of the transition dipole from the excited state (the superscript e) of the donor molecule to its ground state (the superscript g). The matrix elements of the electric dipole-dipole coupling tensor $\overleftrightarrow{\theta}(\omega, \mathbf{r_D}, \mathbf{r_A})$ in vacuum are[51–58]

$$\begin{aligned}&\theta_{ij}(\omega, \mathbf{r_D}, \mathbf{r_A})\\ &= \frac{\omega^3 e^{i\omega R/c}}{4\pi\epsilon_0 c^3}\left[(\delta_{ij} - 3\mathrm{e}_{\mathrm{R}i}\mathrm{e}_{\mathrm{R}j})\left(\frac{c^3}{\omega^3 R^3} - \frac{ic^2}{\omega^2 R^2}\right)\right.\\ &\left.-(\delta_{ij} - \mathrm{e}_{\mathrm{R}i}\mathrm{e}_{\mathrm{R}j})\frac{c}{\omega R}\right]. \qquad (3)\end{aligned}$$

In the equation above, δ denotes the Kronecker delta, $R = |\mathbf{R}| = |\mathbf{r_A} - \mathbf{r_D}|$ is the amplitude of the displacement vector between the donor and the acceptor, and $\mathrm{e}_{\mathrm{R}i}$ stands for the i-th component of the unit vector of $\mathbf{R}$ ($\mathbf{e_R} = \mathbf{R}/R$). It is clear from Eqs. (3) and (1) that $|M(\omega, \mathbf{r_D}, \mathbf{r_A})|^2$ and the RET rate $k_{D\to A}(\omega)$ both have an inverse sixth-power distance dependence in the near-zone ($\omega R/c \ll 1$), and an inverse quadratic dependence in the far-zone ($\omega R/c \gg 1$). Eq. (3) is restricted to RET in homogeneous and non-absorbing media, i.e., the index of refraction is a real number and it is independent of $\mathbf{r}$ and ω. Through the years, several studies have successfully described RET in inhomogeneous or periodic media using computational chemistry techniques[59,60] or QED[61], but these methods cannot adequately describe the behavior of PC-RET because the index of refraction needs to be represented as both a space- and frequency-dependent complex function in the theory. Recently, some theoretical studies have been done for treating RET in absorbing and dispersive[55,62–64] media by calculating the dyadic Greens function, and computational methods have been developed to describe emission and radiative decay rates in the vicinity of a variety of structures, including dielectric interfaces,[65–67] planar dielectric/metallic surfaces,[68–70] cavities between plates or mirrors,[71–76] spherical cavities,[77,78] multilayer geometries,[79] nanoparticles (such as nanospheres[80,81], nanorods[82–86], and other more complex structures[87]), and photonic crystals.[76,88–92] Most of these methodologies involve imposing specific boundary conditions on the electromagnetic fields to simplify the analysis, and are unable to treat arbitary environments.

Here, we present a general but simple computational scheme, termed the time-domain electrodynamics resonance energy transfer (TED-RET) method, to simulate RET in inhomogenous media. In section II, we show that the transition matrix element for RET ($M(\omega, \mathbf{r_D}, \mathbf{r_A})$) can be expressed in terms of the the donor and acceptor transition moments, and the external polarization field generated by the donor molecule, evaluated at the acceptor molecule. These physical quantities can be obtained using excited state electronic structure methods to evaluate transition moments, and using the finite-difference time-domain (FDTD) method to determine electromagnetic fields. In section III A, the rate of RET in homogeneous media obtained from our method is shown to be exactly the same as the analytic solution from quantum electrodynamics. To demonstrate the broad applicability of the present approach, in sections III B and III C, we study PC-RET in the vicinity of gold nanoparticles and show that the plasmonic enhancement factor (PEF) for RET, compared to the vacuum value, can be as high as 10^6.

II. METHODS

A. Theory

In this paper, we focus on PC-RET between two molecules (donor and acceptor) in the presence of dispersive and absorbing media and assume no charges and currents embedded in the background dielectrics. There are two crucial steps in the derivation of our theory. First, from classical electrodynamics, we show the relationship between the electric field generated from the donor and the dyadic Greens function (See Eq. (12)). Second, from quantum electrodynamics, the rate of resonance energy transfer can be expressed in terms of the dyadic Greens function (See Eq. (13)). Based on the two results, one can directly compute the rate of resonance energy transfer using real-time classical electrodynamics methods instead of solving the dyadic Greens function. For applications to energy transfer in inhomogeneous, absorbing, and dispersive environments, this has significant computational advantages.

We start from classical electrodynamics. In inhomogeneous dispersive and absorbing media, the electromagnetic fields can be described by Maxwell's equations

$$\nabla \cdot \mathbf{D}(\mathbf{r}, t) = 0, \qquad (4a)$$

$$\nabla \cdot \mathbf{B}(\mathbf{r}, t) = 0, \qquad (4b)$$

$$\nabla \times \mathbf{E}(\mathbf{r}, t) = -\frac{\partial \mathbf{B}(\mathbf{r}, t)}{\partial t}, \qquad (4c)$$

$$\nabla \times \mathbf{H}(\mathbf{r}, t) = \frac{\partial \mathbf{D}(\mathbf{r}, t)}{\partial t}. \qquad (4d)$$

For a dielectric medium with permeability μ, we have

$$\mathbf{B}(\mathbf{r}, t) = \mu \mathbf{H}(\mathbf{r}, t), \qquad (5a)$$

$$\mathbf{D}(\mathbf{r}, t) = \mathbf{D}_{\mathrm{med}}(\mathbf{r}, t) + \mathbf{P}_{\mathrm{ex}}(\mathbf{r}, t), \qquad (5b)$$

where the magnetic field $\mathbf{B}(\mathbf{r}, t)$ is proportional to the demagnetizing field $\mathbf{H}(\mathbf{r}, t)$, and the total displacement field $\mathbf{D}(\mathbf{r}, t)$ includes the displacement field of the inhomogeneous media $\mathbf{D}_{\mathrm{med}}(\mathbf{r}, t)$ and the external polarization generated by a donor molecule $\mathbf{P}_{\mathrm{ex}}(\mathbf{r}, t)$. Here, we consider RET in the vicinity of gold nanoparticles so it is adequate to assume that $\mu \approx \mu_0$ (the vacuum permeability). In fact this assumption can be applied to any material with a relative permeability close to 1, such as water, silver, copper, etc.

By using Eqs. (4) – (5), Maxwell's equations can be cast into an inhomogeneous partial differential equation:

$$-\left(\mu_0\frac{\partial^2\mathbf{D}_{\mathrm{med}}(\mathbf{r},t)}{\partial t^2}+\nabla\times\{\nabla\times\mathbf{E}(\mathbf{r},t)\}\right)$$
$$=\mu_0\frac{\partial^2\mathbf{P}_{\mathrm{ex}}(\mathbf{r},t)}{\partial t^2}. \tag{6}$$

Considering that a single radiating donor molecule is at $\mathbf{r}_{\mathbf{D}}$ and the molecular size is much smaller than the distance between the donor and the acceptor, it is appropriate to make the point-dipole approximation and assume that $\mathbf{P}_{\mathrm{ex}}(\mathbf{r},t)=\mathbf{p}_{\mathrm{ex}}(t)\delta(\mathbf{r}-\mathbf{r}_{\mathbf{D}})$. Moreover, assume that the background medium as a linear time-invariant medium $\mathbf{D}_{\mathrm{med}}(\mathbf{r},\omega)=\epsilon_r(\mathbf{r},\omega)\epsilon_0\mathbf{E}(\mathbf{r},\omega)$, after performing the temporal Fourier transform, Eq. (6) in the frequency domain is

$$\left(\frac{\epsilon_r(\mathbf{r},\omega)\omega^2}{c^2}\mathbf{E}(\mathbf{r},\omega)-\nabla\times\{\nabla\times\mathbf{E}(\mathbf{r},\omega)\}\right)$$
$$=\frac{-\omega^2}{c^2\epsilon_0}\mathbf{p}_{\mathrm{ex}}(\omega)\delta(\mathbf{r}-\mathbf{r}_{\mathbf{D}}), \tag{7}$$

where the speed of light in vacuum $c=1/\sqrt{\epsilon_0\mu_0}$ and $\mathbf{p}_{\mathrm{ex}}(\omega)=F\{\mathbf{p}_{\mathrm{ex}}(t)\}$ (the temporal Fourier transform of $\mathbf{p}_{\mathrm{ex}}(t)$). Note that the index of refraction $n(\mathbf{r},\omega)=\sqrt{\epsilon_r(\mathbf{r},\omega)}$ is a complex function, and this leads to screening of the dipole in the presence of a dielectric medium, as is appropriate[55,93]. The related issue of local field scaling of the dipole will be addressed in the Conclusion. The solution of Eq. (7) can be expressed in terms of the dyadic Green's function $\overleftrightarrow{g}(\mathbf{r},\mathbf{r}',\omega)$ and it consists of two terms,

$$\mathbf{E}(\mathbf{r},\omega)$$
$$=\mathbf{E}^{(0)}(\mathbf{r},\omega)+\int\overleftrightarrow{g}(\mathbf{r},\mathbf{r}',\omega)\left(-\frac{\omega^2}{c^2\epsilon_0}\right)\mathbf{p}_{\mathrm{ex}}(\omega)\delta(\mathbf{r}'-\mathbf{r}_{\mathbf{D}})d\mathbf{r}'$$
$$=\mathbf{E}^{(0)}(\mathbf{r},\omega)+\overleftrightarrow{g}(\mathbf{r},\mathbf{r}_{\mathbf{D}},\omega)\left(-\frac{\omega^2}{c^2\epsilon_0}\right)\mathbf{p}_{\mathrm{ex}}(\omega), \tag{8}$$

where $\overleftrightarrow{g}(\mathbf{r},\mathbf{r}',\omega)$ satisfies

$$\left(\frac{\epsilon_r(\mathbf{r},\omega)\omega^2}{c^2}-\nabla\times\nabla\times\right)\overleftrightarrow{g}(\mathbf{r},\mathbf{r}',\omega)=-\delta(\mathbf{r}-\mathbf{r}'). \tag{9}$$

In Eq. (8), the first term $\mathbf{E}^{(0)}(\mathbf{r},\omega)$ is the homogeneous solution of Eq. (7), and the second term corresponds to the inhomogeneous solution (a response caused by the external polarization field). Note that we assume that $\epsilon_r(\mathbf{r},\omega)$ is independent of the positions of the molecules, i.e., we neglect the influence of the molecules on the dielectrics. We rearrange the terms in Eq. (8) and it becomes

$$\mathbf{E}^{\mathrm{D}}(\mathbf{r}_{\mathbf{A}},\omega)=-\frac{\omega^2}{c^2\epsilon_0}\overleftrightarrow{g}(\mathbf{r}_{\mathbf{A}},\mathbf{r}_{\mathbf{D}},\omega)\mathbf{p}_{\mathrm{ex}}(\omega), \tag{10}$$

where we define a response electric field at $\mathbf{r}_{\mathbf{A}}$ (the position of the acceptor molecule) caused by the donor molecule as

$$\mathbf{E}^{\mathrm{D}}(\mathbf{r}_{\mathbf{A}},\omega)=\mathbf{E}(\mathbf{r}_{\mathbf{A}},\omega)-\mathbf{E}^{(0)}(\mathbf{r}_{\mathbf{A}},\omega). \tag{11}$$

Note that we assume that there is no internal electric field in the inhomogeneous media in our simulations (that is, $\mathbf{E}^{(0)}(\mathbf{r}_{\mathbf{A}},\omega)=0$), but Eq. (10) can be generally applied to inhomogeneous media with internal electric fields.

Taking an inner product of Eq. (10) and $\mathbf{e}_{\mathbf{A}}$ (the unit vector of the transition dipole of the acceptor molecule) and letting $\mathbf{p}_{\mathrm{ex}}(\omega)=\mathrm{p}_{\mathrm{ex}}(\omega)\mathbf{e}_{\mathbf{D}}$, where $\mathbf{e}_{\mathbf{D}}$ is the unit vector of the transition dipole of the donor molecule, Eq. (10) becomes

$$-\frac{\mathbf{e}_{\mathbf{A}}\cdot\mathbf{E}^{\mathrm{D}}(\mathbf{r}_{\mathbf{A}},\omega)}{\mathrm{p}_{\mathrm{ex}}(\omega)}=\frac{\omega^2}{c^2\epsilon_0}\mathbf{e}_{\mathbf{A}}\overleftrightarrow{g}(\mathbf{r}_{\mathbf{A}},\mathbf{r}_{\mathbf{D}},\omega)\mathbf{e}_{\mathbf{D}}. \tag{12}$$

Eq. (12) clear shows the relationship between the electric field generated by a donor molecule and the dyadic Greens function. Here we recall that the external polarization is generated by the donor molecule so the external polarization and the transition dipole of the donor molecule have the same unit vector $\mathbf{e}_{\mathbf{D}}$.

For absorbing and dispersive media, in the framework of quantum electrodynamics and Fermi's golden rule, the transition matrix has been found can be expressed as follows[64],

$$M(\omega,\mathbf{r}_{\mathbf{D}},\mathbf{r}_{\mathbf{A}})=\mu^{eg}(\mathbf{r}_{\mathbf{A}})\mu^{ge}(\mathbf{r}_{\mathbf{D}})\frac{\omega^2}{c^2\epsilon_0}\mathbf{e}_{\mathbf{A}}\overleftrightarrow{g}(\mathbf{r}_{\mathbf{A}},\mathbf{r}_{\mathbf{D}},\omega)\mathbf{e}_{\mathbf{D}}, \tag{13}$$

where $\mu^{ge}(\mathbf{r}_{\mathbf{D}})$ ($\mu^{eg}(\mathbf{r}_{\mathbf{A}})$) stands for the magnitude of the transition dipole of the donor (acceptor) molecule, and $\mu^{ge}(\mathbf{r}_{\mathbf{D}})$ represents the transition dipole from the excited state (the superscript e) of the donor molecule to its ground state (the superscript g). Comparing Eq. (12) with Eq. (13), we obtain the final result

$$M(\omega,\mathbf{r}_{\mathbf{D}},\mathbf{r}_{\mathbf{A}})=-\mu^{eg}(\mathbf{r}_{\mathbf{A}})\mu^{ge}(\mathbf{r}_{\mathbf{D}})\frac{\mathbf{e}_{\mathbf{A}}\cdot\mathbf{E}^{\mathrm{D}}(\mathbf{r}_{\mathbf{A}},\omega)}{\mathrm{p}_{\mathrm{ex}}(\omega)}. \tag{14}$$

Here, we would like to emphasize that Eq. (14) provides a convenient and direct computational scheme for studying resonance energy transfer in inhomogeneous and absorbing media because (i) $\mathbf{E}^{\mathbf{D}}(\mathbf{r}_{\mathbf{A}},\omega)$ and $\mathrm{p}_{\mathrm{ex}}(\omega)$ can be obtained from computational electromagnetics software based on the FDTD method, (ii) $\mu^{eg}(\mathbf{r}_{\mathbf{A}})$ and $\mu^{ge}(\mathbf{r}_{\mathbf{D}})$ can be calculated via quantum chemistry software based on excited state methods, e.g., time-dependent density functional theory, (iii) Eq. (14) can be applied to dispersive and absorbing media, not limited to inhomogeneous media, and (iv) the validity of Eq. (14) is independent of the shape of the dielectrics. In other words, this formula can be applied to studying RET in inhomogeneous absorbing and dispersive media based on any type of nanostructure that is weakly-coupled to the electromagnetic fields and with relative permeability close to 1. Note that $M(\omega,\mathbf{r}_{\mathbf{D}},\mathbf{r}_{\mathbf{A}})$ and $\mathbf{E}^{\mathbf{D}}(\mathbf{r}_{\mathbf{A}},\omega)$ can be complex functions because $\mathbf{E}^{\mathbf{D}}(\mathbf{r}_{\mathbf{A}},\omega)$ is the Fourier transform of a real function $\mathbf{E}(\mathbf{r}_{\mathbf{A}},t)$ (recall that we let $\mathbf{E}^{(0)}(\mathbf{r}_{\mathbf{A}},t)=0$).

B. Simulation details

In order to capture the properties of real molecules in applications of the RT-ED-RET approach, we calculated the transition dipole moment between the S_0 and S_1 states of 6 molecules in the acene family, as their RET properties (up to pentacene) are well studied. For the ground state geometry optimization and the calculation of S_0-S_1 transition dipole, we used the NWChem computational package,[94] with exchange-correlation PBE0 functional[95] and cc-pVDZ basis set.[96] We used density functional theory (DFT) for the ground state optimization, while excited state calculations were performed with time-dependent density functional theory (TDDFT). The identities of these molecules are presented in Table I, together with their $S_0 - S_1$ transition dipole moment and excitation energy. All of these molecules have a transition dipole moment amplitude close to 1 a.u.. Therefore, in all following FDTD simulations, we chose $\mu^{eg}(\mathbf{r_A}) = \mu^{ge}(\mathbf{r_D}) = 1$ a.u. uniformly for simplicity. The excitation energies in Table I for the $S_0 - S_1$ transitions are spread across the visible-near IR spectrum. Hence, to achieve maximum plasmonic effect, we have used the wavelength of the absorption maximum of each nanoparticle as ω in Eq. 14 for the FDTD calculations, rather than the actual excitation energy of a specific molecule. The actual wavelengths used for nanoparticles will be listed in later sections.

The calculations of $\mathbf{E^D}(\mathbf{r_A}, \omega)$ were performed by the computational package Lumerical FDTD Solutions,[97] a commercial-grade simulator based on the finite-difference time-domain method. Several different systems were considered in our study, whose geometry setup will be described in detail in the following sections together with the presentation and discussion of their results. In this section, we provide the general parameters and settings used in these calculations. All simulations were set to run for 100 fs, with some of them terminating earlier when they reached the auto-shutoff parameter (the fraction of the field intensity that is still in the simulation box) of 10^{-7}. All boundaries are set to be perfectly matched layers (PML). Symmetry was used along the Y and Z directions to minimize computational cost. The donor molecule was approximated as an oscillating electric point dipole source with a wavelength at the absorption maximum of the accompanied nanoparticle, and a polarization direction as specified later. Other parameters of the dipole were kept the same as the default, unless otherwise stated. The dielectric function of gold from Johnson and Christy[98] was used for any gold nanoparticle included in the simulation. For the cases considered in section III A, a FDTD domain of 2000 × 1100 × 1100 nm was used. A conformal mesh of 1 nm was imposed on the region of 613 × 10 × 10 nm covering the dipole source and the monitor range, while the outside mesh was chosen to be auto-nonuniform with a mesh accuracy of 4 (a setting in the Lumerical FDTD Solution). For the nanosphere cases in section III B, the sides of the FDTD domain for each case considered are set to at least 20 times the sphere's diameter. A conformal mesh was applied to the space containing the nanosphere, with each side of the cubic space to be 20 nm larger than the sphere diameter. The grid size was chosen to be 1/400 of the sphere diameter, while the outside grid size was set to be auto-nonuniform with a mesh accuracy of 4. For nanorod cases in section III C, the FDTD domain was selected such that each side of the domain was 1 μm larger than the corresponding side of the rod. The region between the donor molecule (source) and 5 nm into the nanorod, as well as between any acceptor molecule (monitor) and 5 nm into the nanorod, has a mesh of 0.2 nm; while the rest of the nanorod was covered with a mesh of 1% of the corresponding rod size. Outside these mesh override regions, the same auto-nonuniform mesh setting was in effect, with a mesh accuracy of 4.

III. RESULTS AND DISCUSSION

In this section, three different systems are considered, namely the homogeneous media in section III A, gold nanospheres in section III B, and gold nanorods in section III C. Calculated values of the transition matrix element $M(\omega, \mathbf{r_D}, \mathbf{r_A})$ in these different cases will be presented, and the plasmonic enhancement factor (PEF) will be analyzed and discussed.

A. Homogeneous media

Here we show that the transition matrix element computed using our method is the same as the analytic solution from quantum electrodynamics, and we study variation of the results with respect to numerical parameters in the theory. We tested eleven cases with different settings, nine of which are in vacuum, one in water, and one in an arbitrary dielectric medium. For all cases, the donor in RET was simulated by using an oscillating electric point dipole polarized in the Z direction at the origin, while the acceptor was a second electric dipole with equal magnitude and polarization as the donor, located on the X-axis and separated from the donor by a distance R (i.e. $\mathbf{r_D} = (0,0,0)$ and $\mathbf{r_A} = (R,0,0)$). As stated in the section II B, the amplitudes of all donor and acceptor transition dipoles were set to 1 a.u.. Hence, in homogeneous media with a constant relative permittivity ϵ_r, the transition matrix element in atomic units becomes:

$$M_{ZZ}(\omega, \mathbf{r_D}, \mathbf{r_A}) = \frac{\omega^3 e^{i\omega R/c'}}{4\pi\epsilon_0\epsilon_r c'^3}\left(\frac{c'^3}{\omega^3 R^3} - \frac{ic'^2}{\omega^2 R^2} - \frac{c'}{\omega R}\right), \tag{15}$$

where c' is the speed of light in the host media, $c' = c/\sqrt{\epsilon_r}$. Since the electric dipole source takes the form of a pulse signal, the nine vacuum cases were used to con-

TABLE I. Acene molecules and their structures with their $S_0 - S_1$ transition dipole moment amplitude in atomic units and excitation energy in wavelength.

Molecule	**Structure**	**Transition dipole moment** (a.u.)	**Excitation energy** (nm)
Naphthalene	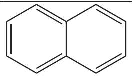	0.75638	275
Anthracene	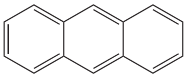	0.86480	374
Tetracene	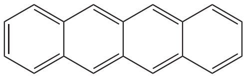	0.91574	491
Pentacene	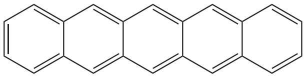	0.94884	630
Hexacene	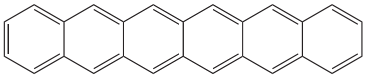	0.96932	794
Heptacene	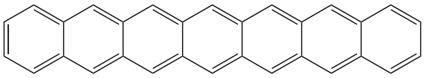	0.97853	989

firm that our approach is robust under different source wavelengths and pulse lengths, while the water and dielectric medium cases were used to test the method for the non-vacuum host media.

For the vacuum cases, we chose three different wavelengths (λ) as the dipole source oscillation frequency, and for each wavelength, three different pulse lengths T_{pulse} were tested. The source time signal $\mathrm{p_{ex}}(t)$ generated by the donor molecule is chosen as:

$$\mathrm{p_{ex}}(t) = \sin\left[-\omega(t-t_0)+\frac{\pi}{2}\right] e^{-\frac{(t-t_0)^2}{2\Delta t^2}} \tag{16}$$

where $\omega = 2\pi c/\lambda$ is the angular frequency of the source, t_0 is the pulse delay time selected to ensure that the wave envelope starts after $t = 0$, and the standard deviation Δt defines the width of the Gaussian envelope and is related to the pulse length by $\Delta t = T_{pulse}/\left[2\sqrt{\ln(2)}\right]$ as defined in the Lumerical FDTD Solution package. To avoid systematic error, the three wavelengths were chosen to be 300 nm, 491 nm, and 720 nm; with non-uniform intervals. The program default pulse lengths were: 1.98157 fs for 300 nm source, 3.24365 fs for 491 nm source, and 4.75577 fs for 720 nm source. Although Δt, and hence the pulse lengths, were different in each case, they were scaled so that the number of cycles within each pulse was the same. The other two pulse lengths tested for each source wavelength were set to be twice and thrice the default pulse length, therefore doubling and tripling the number of cycles within the pulse, respectively. The source time signals of all nine vacuum cases are shown in Fig. 1, with the appropriate label for their corresponding wavelength λ and standard deviation Δt on top of each graph. The numerical results from FDTD and the corresponding analytical results, are presented in Fig. 2. The figures show the real and imaginary parts of the transition matrix element $M(\omega, \mathbf{r_D}, \mathbf{r_A})$ between donor and acceptor, as the acceptor moves along the X direction. As one can see, for each case, the real part of the FDTD result (solid green) matches that of the analytic solution (dashed red), and so does the imaginary part (solid cyan for FDTD and dashed blue for analytic solution). Meanwhile, within each group with the same wavelength, the results do not change as the pulse length changes. Thus, we conclude that our numerical method for calculating $M(\omega, \mathbf{r_D}, \mathbf{r_A})$ is robust for a variety of source wavelengths and pulse lengths.

After validation of the vacuum cases, we moved on to the non-vacuum cases. Setting the source to be λ=491 nm and Δt=1.948010 fs, we defined the host environment to be either water with relative permittivity ϵ_r=1.796 or a dielectric medium with ϵ_r=5. After performing the same calculations as in the vacuum cases, we obtained the results shown in Fig. 3. Once again, the real and imaginary parts from the two methods match each other, respectively. Furthermore, as expected, one observes different distance-dependent oscillations of the real and imaginary parts of $M(\omega, \mathbf{r_D}, \mathbf{r_A})$ in vacuum, water, and ϵ_r=5 dielectric medium. Even though the source is kept the same, the period of this oscillation is determined by the exponential term $e^{i\omega R/c'}$ in Eq. (15). Since larger permittivity of the host medium leads to a slower speed of light in that medium, the power of the exponential term increases in non-vacuum media, resulting in a smaller spatial oscillation period of $M(\omega, \mathbf{r_D}, \mathbf{r_A})$. Note, however, that even though the real and imaginary parts of $M(\omega, \mathbf{r_D}, \mathbf{r_A})$ oscillate with distance, the rate of RET $k_{D\rightarrow A}(\omega)$ does not. The rate itself will follow R^{-6} in the near-zone and the R^{-2} in the far-zone, because $k_{D\rightarrow A}(\omega)$

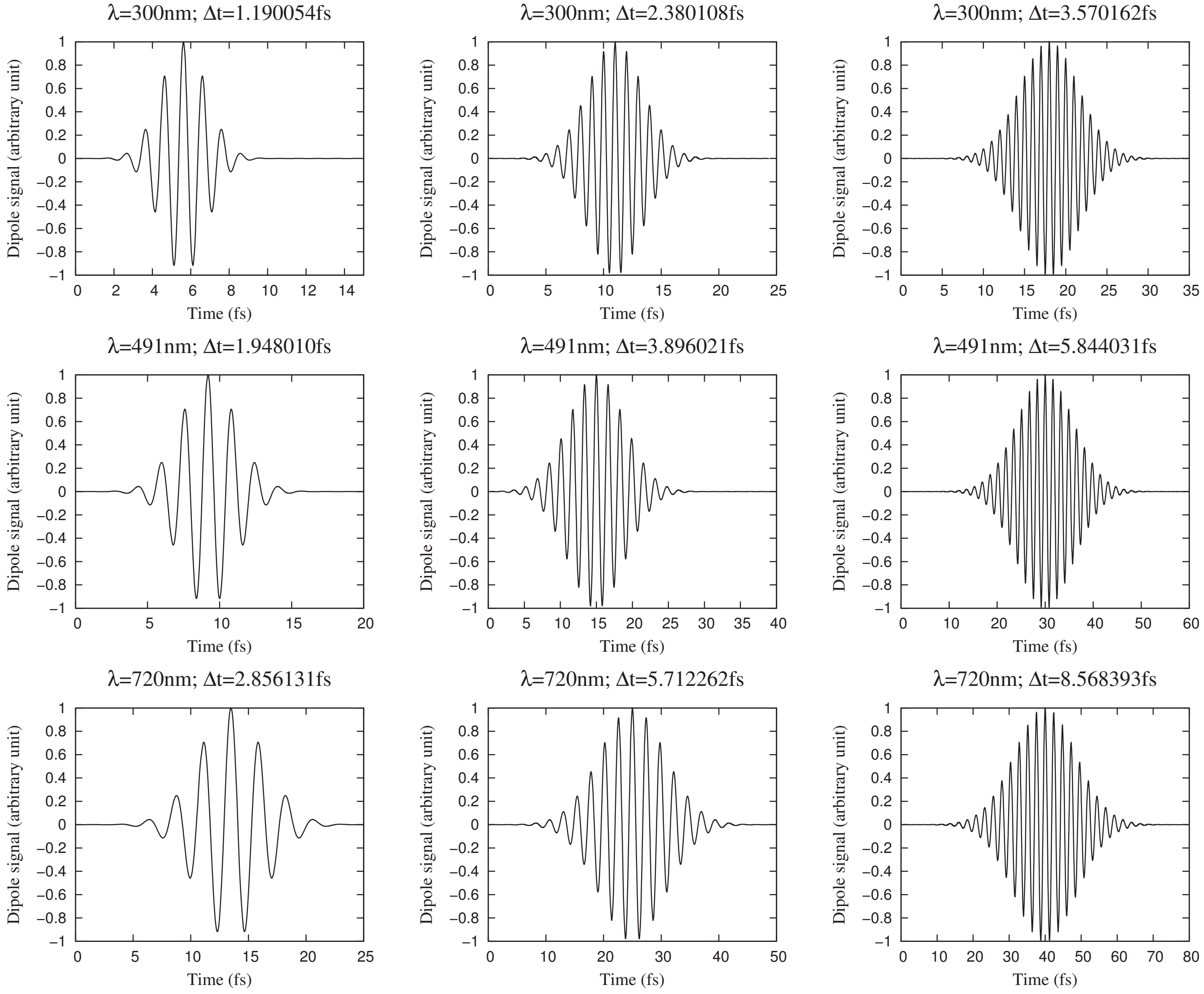

FIG. 1. The source time signals for the nine vacuum cases, labeled with their corresponding wavelength λ and standard deviation Δt. Figures in the same row have the same wavelength, but different pulse lengths.

is proportional to the absolute square of $M(\omega, \mathbf{r_D}, \mathbf{r_A})$, i.e., $|M(\omega, \mathbf{r_D}, \mathbf{r_A})|^2$.

To summarize, the proposed computational scheme using the FDTD method leads to reliable RET rates in homogeneous media. It is robust under a variety of choices of source wavelength, pulse length, and permittivity of the host media. Therefore, it can be confidently applied to more complex environments, as we shall demonstrate in the following sections, with examples where RET occurs in the presence of gold nanospheres and nanorods with different sizes.

B. Gold nanospheres

A total of five gold nanospheres were chosen for this study, with diameters of 10, 25, 50, 75, and 100 nm. The setup showing the relative positions of the nanospheres and the dipoles is presented in Fig. 4(a), where the solid double-arrow represents the donor molecule with a transition dipole, while the dashed arrows are the acceptors at different locations on the particle surface. The donor and the acceptor, together with the nanospheres, are taken to be in vacuum . All donor and acceptor molecules were approximated by point dipoles that were 5 nm from the surfaces of the nanospheres, regardless of the diameters of the spheres. This choice was made to avoid potential charge transfer between molecules and the gold particles that would be associated with smaller separations. The

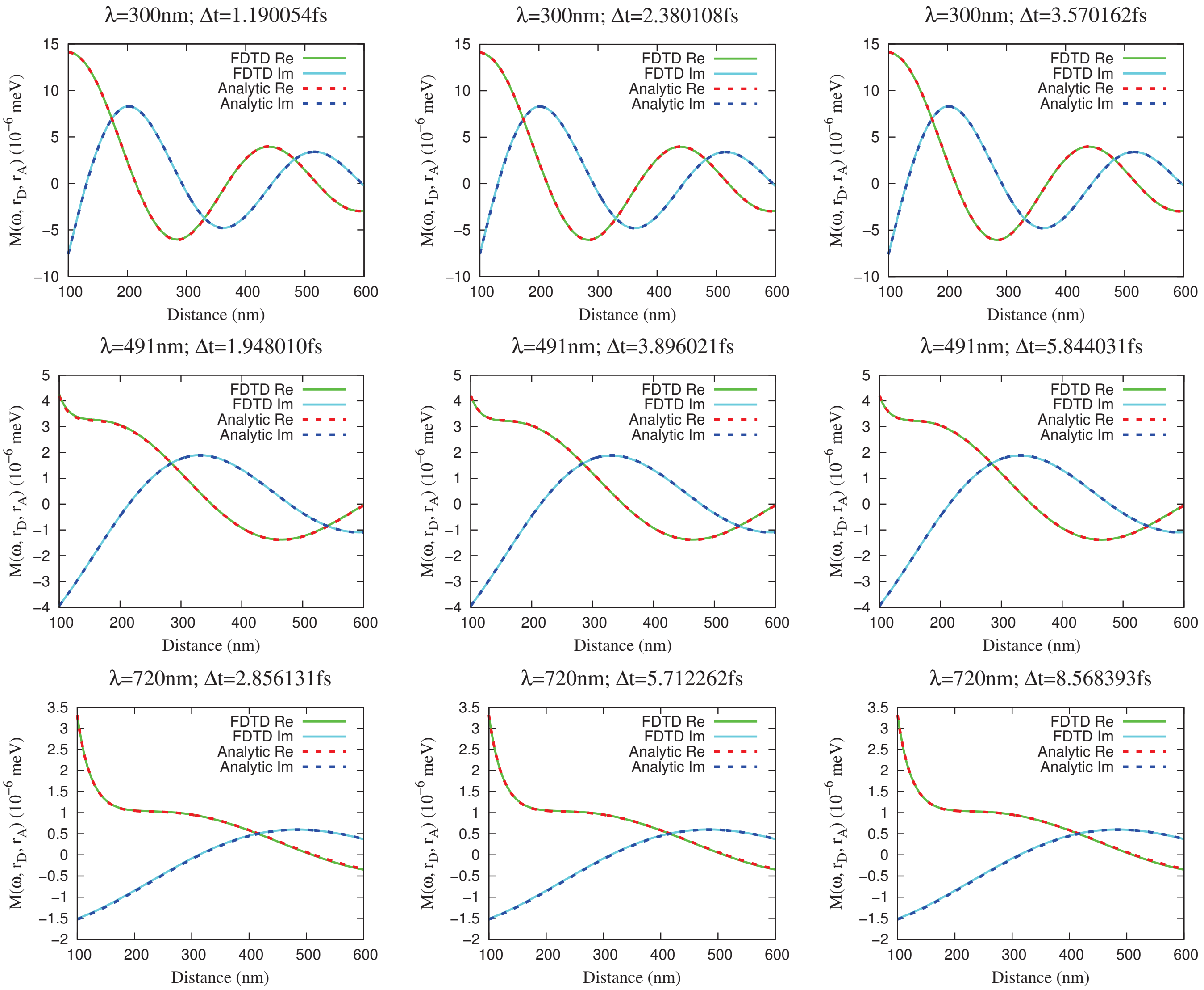

λ=300nm; Δt=1.190054fs

λ=300nm; Δt=2.380108fs

λ=300nm; Δt=3.570162fs

λ=491nm; Δt=1.948010fs

λ=491nm; Δt=3.896021fs

λ=491nm; Δt=5.844031fs

λ=720nm; Δt=2.856131fs

λ=720nm; Δt=5.712262fs

λ=720nm; Δt=8.568393fs

FIG. 2. Comparison between FDTD results and analytic solution for the vacuum cases, labeled with their corresponding wavelength λ and standard deviation Δt. In each graph, the solid green and cyan lines are the real and imaginary parts of the FDTD result, respectively; while the dashed red and blue lines are the real and imaginary parts of the analytic solution. The real parts from the FDTD and analytic solutions match each other, and so do the imaginary parts.

polarization directions of the dipoles were assumed pointing radially towards the center of the nanosphere, so as to mimic molecules in which the transition dipoles are oriented with a similar local geometry at each point on the surface. A total of 12 positions were examined, mapping out a semicircle on the particle surface. An angle ϕ can be defined by the line from the donor point dipole to the nanosphere center and the line from the acceptor to the center. These 12 positions were chosen so that the angle ϕ in the figure has an increment of 15° as the acceptor maps out the semicircle. Please note that even though 12 dashed arrows are shown in the figure and only one FDTD simulation is needed to calculate the electric field at all desired positions, only one acceptor is included in each RET rate calculation.

The normalized absorption spectra for all the spheres considered are shown in Fig. 4(b). As mentioned in section II B, the wavelength of the absorption maximum for each nanoparticle was used for the RET calculations. These wavelengths are: $\omega = 506$ nm for the 10 nm and 25 nm spheres, 508 nm for the 50 nm sphere, 511 nm for the 75 nm sphere, and 515 nm for the 100 nm sphere. For each nanosphere, the electric field generated from the donor dipole source was calculated for both cases with and without the nanosphere present. Setting the acceptor dipoles with the same amplitude as the donor, $|M(\omega, \mathbf{r_D}, \mathbf{r_A})|^2$ was obtained for all the desired locations on the particle surface. The results are shown in the log

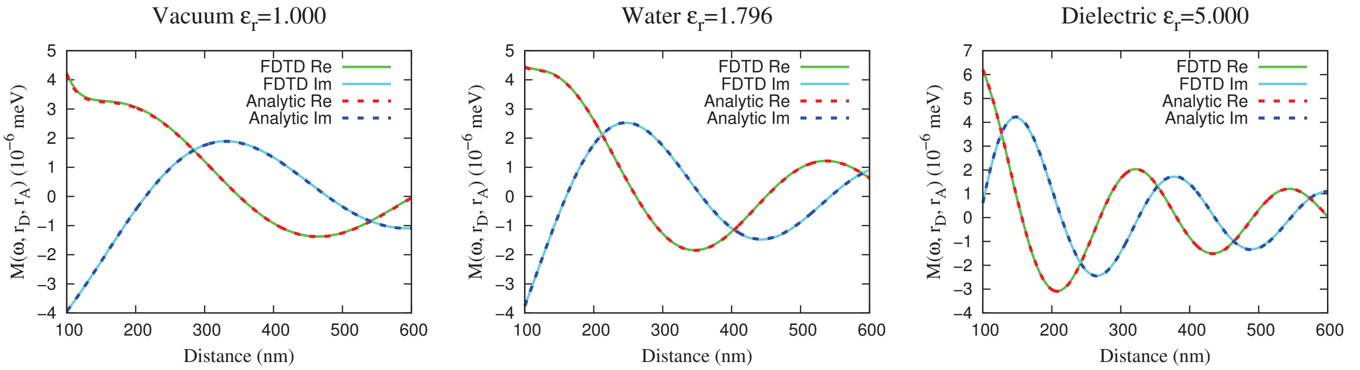

FIG. 3. Comparison between FDTD results and analytic solution for the dielectric medium cases, labeled with their corresponding relative permittivity ϵ_r. In each graph, the solid green and cyan lines are the real and imaginary parts of the FDTD results, respectively; while the dashed red and blue lines are the real and imaginary parts of the analytic solution. The results show that the real parts from FDTD and analytic solutions match each other precisely, and so do the imaginary parts.

plot in Fig. 4(c), with the PEF results being in (d). Here the PEFs are the ratios of $|M(\omega, \mathbf{r_D}, \mathbf{r_A})|^2$ from the cases with nanosphere and their counterpart from the vacuum cases. As one can see, the PEF can be enhanced by 2 orders of magnitude in the presence of nanospheres, depending on the positions of the donor and the acceptor relative to the nanoparticles.

For all cases, maximum enhancement is achieved when the donor and the acceptor are separated by the entire nanoparticle. This arises because the polarization direction of the acceptor dipole is completely aligned with that of the dipolar plasmon resonance of the nanosphere. Meanwhile, not only does the 100 nm nanosphere case show the largest enhancement, the values of $|M(\omega, \mathbf{r_D}, \mathbf{r_A})|^2$ at positions with $\phi \geq 115°$ in the 100 nm case are larger than those in the 50 and 75 nm vacuum cases. Even though these values are still smaller than those in the other two vacuum cases, the differences decrease from 3 or 4 orders of magnitude to within 1 or 2 orders of magnitude, for 25 and 10 nm cases respectively. This demonstrates great potential for the plasmonic nanospheres to be useful in in RET, as they not only enhance the transfer rate, but also reduce the long-range decay of the rate.

It is worth noting that the RET is not always enhanced by plasmonic effects in the simulations. Fig. 4(d) shows that the PEFs are mostly less than 1 when $\phi \leq 30°$, and for the 10 and 25 nm cases, even the 45° position has a PEF smaller than 1. This means that the value of $|M(\omega, \mathbf{r_D}, \mathbf{r_A})|^2$ is suppressed in the presence of nanospheres compared to that in vacuum. This suppression arises from interference between the dipole electric field from the donor and the induced dipole electric field from the nanosphere when both fields are evaluated at the acceptor. This is because the donor and acceptor are in an H-aggregate geometry[99] for small ϕ where the field of the donor points oppositely to the donor direction when evaluated at the acceptor, while the donor-particle and particle-acceptor geometries are both J-aggregate in character, meaning that the induced field is parallel to the donor dipole when evaluated at the acceptor. As a result of this interference, smaller $|M(\omega, \mathbf{r_D}, \mathbf{r_A})|^2$ values are generated. For larger ϕ, especially $\phi = 180°$, both the donor-acceptor and donor-particle-acceptor interactions have J-aggregate character and the interaction is constructive.

C. Gold nanorods

In a similar fashion, PC-RET was probed for gold nanorods. Here we chose gold nanorods 50 nm in diameter and with lengths such that the aspect ratio (AR) was 1:1, 2:1, 4:1, 6:1, and 8:1, corresponding to rod lengths of 50 nm, 100 nm, 200 nm, 300 nm, and 400 nm, respectively. As shown in Fig. 5(a), the donor dipole was placed at the center of one end of the rod, with a 5 nm distance to the rod surface. Four positions were chosen for the acceptor, namely one at the center of the opposite end of the rod from where the donor is located (position ④), and three positioned at 1/4, 1/2, and 3/4 the rod length from the donor end along the curved surface of the rod (position ①, ②, and ③). All acceptor positions were also separated from the particle surface by 5 nm. The polarizations of all dipoles were perpendicular to the local surface. Again, only one FDTD simulation was needed to obtain the electric field at all acceptor positions, and only one acceptor position was considered in each RET rate calculation.

Fig. 5(b) shows the normalized absorption spectra of the five choices of nanorods with 50 nm diameter and different aspect ratios. We only focused on rods where plasmon resonances are in the visible to near-IR region, corresponding to where the last four molecules in Table I absorb. Similar to the nanosphere cases, we used the wavelength of maximum absorption as the frequency of the dipole source (donor) for each nanorod case to achieve

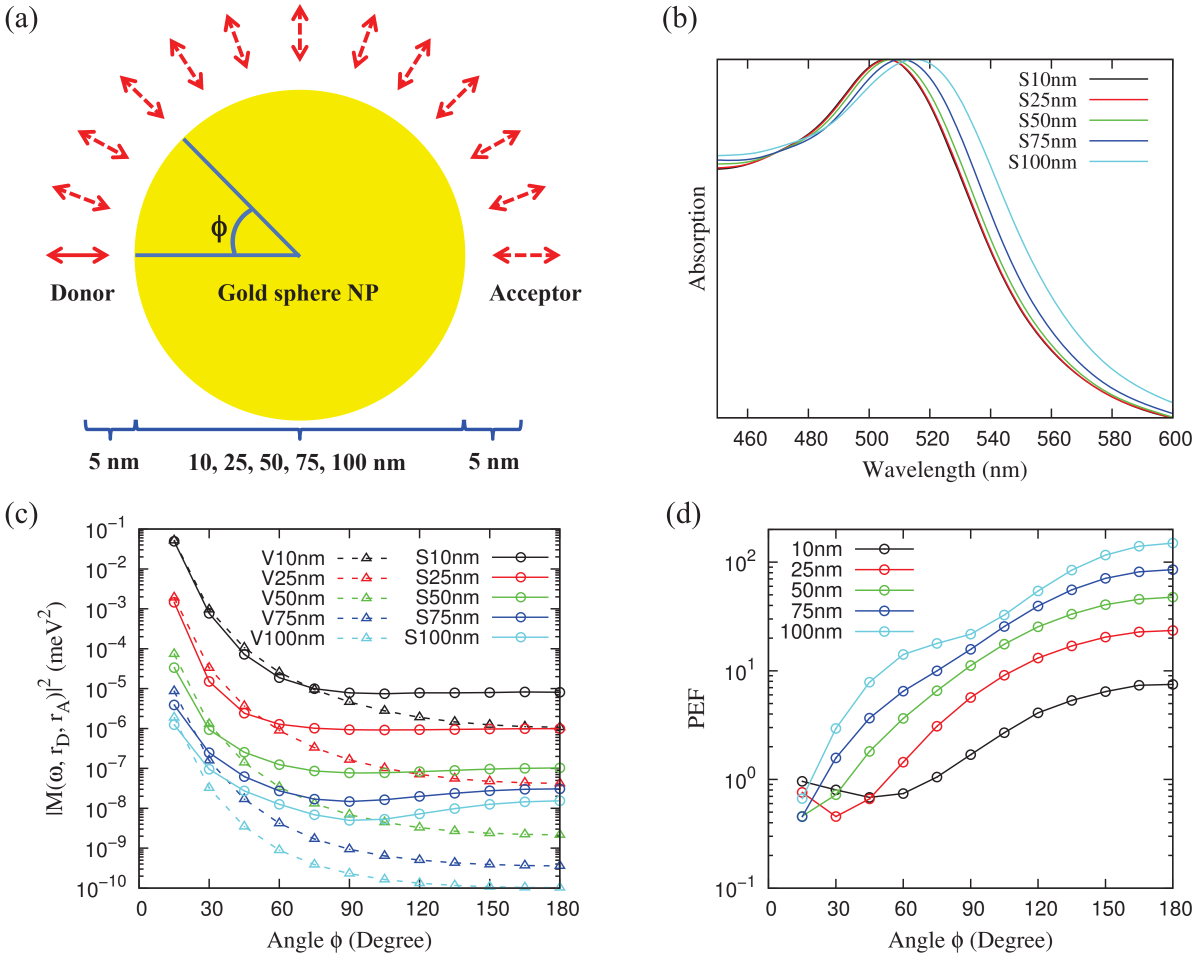

FIG. 4. Geometry setup and simulation results for RET near a gold nanosphere. (a) Relative positions of gold nanosphere and donor-acceptor pair, where the angle ϕ is defined by the line from the donor to the sphere center and the line from the acceptor to the sphere center; (b) the normalized absorption spectra of the different nanospheres; (c) simulation results showing $|M(\omega, \mathbf{r_D}, \mathbf{r_A})|^2$ versus ϕ, with solid lines and the letter "S" representing simulations with the nanospheres, while dashed lines and the letter "V" representing the same calculations but without the nanospheres; (d) PEF of the RET rate, calculated by taking the ratio of $|M(\omega, \mathbf{r_D}, \mathbf{r_A})|^2$ from the nanosphere case and from the vacuum case.

a significant enhancement factor. This wavelength corresponds to the dipole mode of the plasmon resonance in each case, however, other resonance modes can also be excited by a dipole source with appropriate energy and enhance the electric field propagating around the particle. The wavelengths used are: $\omega = 531$ nm for the AR 1:1 case, 606 nm for the 2:1 case, 855 nm for the 4:1 case, 1129 for the 6:1 case, and 1405 nm for the 8:1 case. The results for $|M(\omega, \mathbf{r_D}, \mathbf{r_A})|^2$ and PEF are shown in Fig. 5 (c) and (d), respectively.

Fig. 5 (d) shows that the maximum PEF 10^6, corresponding to the 8:1 AR rod and RET to the more distant acceptor sites (as much as 410 nm donor-acceptor separation). Similar to the nanosphere cases, the enhancement is large when the donor and acceptor are at opposite ends of the nanorod; in other words the acceptor being at position ④. However, the largest enhancement occurs at position ③, even though the polarization of the acceptor at position ④ is parallel to that of the donor and the longitudinal modes of LSPR. Note that $|M(\omega, \mathbf{r_D}, \mathbf{r_A})|^2$ has its lowest value at position ③ in the vacuum cases, but this is not true for the nanorod cases. To understand this, we consider what happens in the electrostatic (near-zone) limit for the vacuum case. In this case, $M(\omega, \mathbf{r_D}, \mathbf{r_A})$ becomes:

$$M(\mathbf{r_D}, \mathbf{r_A}) \\ = \frac{\mu^{eg}(\mathbf{r_A})\mu^{ge}(\mathbf{r_D})}{4\pi\epsilon_0 R^3}\left[(\mathbf{e_D}\cdot\mathbf{e_A}) - 3(\mathbf{e_R}\cdot\mathbf{e_D})(\mathbf{e_R}\cdot\mathbf{e_A})\right]. \tag{17}$$

In this case, $M(\mathbf{r_D}, \mathbf{r_A})$ is no longer ω dependent, and the exponential term $e^{i\omega R/c}$ from Eq. (3) is 1. From Fig. 5(a), one can see that the acceptor dipoles at positions ①, ②, and ③ are perpendicular to the donor,

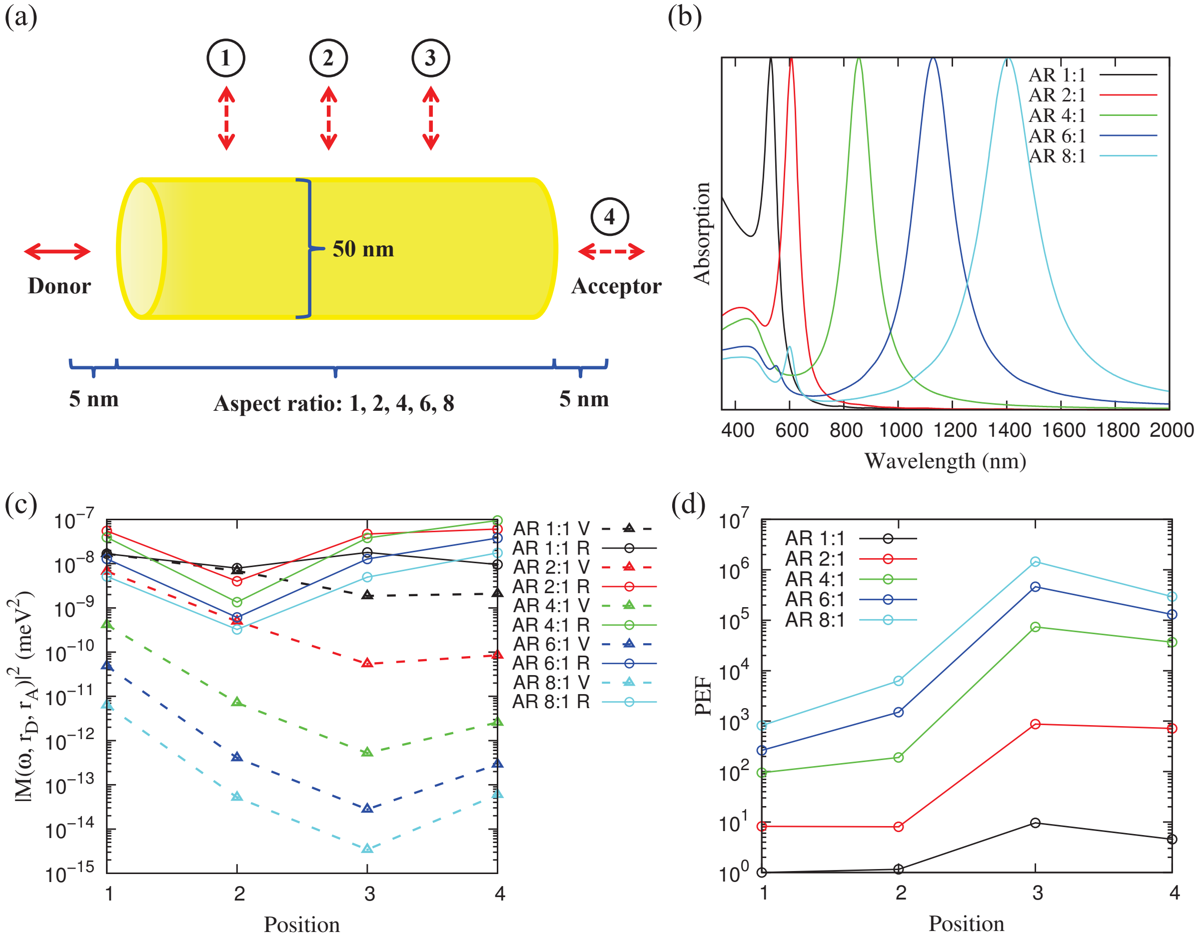

FIG. 5. Geometry setup and simulation results for RET near a gold nanorod. (a) Relative positions of gold nanorod and donor-acceptor pair, the aspect ratio (AR) is calculated by dividing the rod length by the rod diameter; (b) normalized absorption spectra of the different nanorods; (c) simulation results for $|M(\omega, \mathbf{r_D}, \mathbf{r_A})|^2$, with solid lines and the letters "R" representing simulations with nanorods, and dashed lines and letter "V" representing the same calculations but without nanorods; (d) PEF associated with the RET rate, calculated by taking the ratio of $|M(\omega, \mathbf{r_D}, \mathbf{r_A})|^2$ from the nanorod case and from the vacuum case.

and hence, the first term (dot product of two dipoles) in Eq. (17) is zero. The second term depends on the relative positions of the donor and the acceptor as determined by the displacement vector $\mathbf{e_R}$ between the two dipoles. When the acceptor is at positions ① or ②, the angle between the displacement vector and the acceptor dipole vector is still far from being 90°. Thus, $M(\mathbf{r_D}, \mathbf{r_A})$ still has noticeable amplitude. However, at position ③, the large distance between the donor and the acceptor makes the displacement vector much closer to being perpendicular to the acceptor. Therefore, the second term in Eq. (17) is much closer to zero at this point, resulting in a very small $M(\mathbf{r_D}, \mathbf{r_A})$ compared to the other positions. On the other hand, the electric field induced the donor/nanorod interaction involves propagating plasmons on the rod surface that would decay slowly with distance from the donor for lengths considered in this figure, providing a very large enhancement factor at position ③. The slight decrease in enhancement factor at ④ can be understood in terms a loss in propagating plasmon intensity at the end of the smooth nanorod, similar to what was discussed previously with experimental verification.[100]

Of particular significance with respect to the results in Fig. 5 is that because of the large enhancement, the values of $|M(\omega, \mathbf{r_D}, \mathbf{r_A})|^2$ at positions ③ and ④ for all cases are now one order of magnitude larger than those in AR 1:1 case, which in vacuum has the largest values of $|M(\omega, \mathbf{r_D}, \mathbf{r_A})|^2$ because of its shortest length. In fact, from Fig. 5(c), one can see that $|M(\omega, \mathbf{r_D}, \mathbf{r_A})|^2$ has comparable amplitude at all positions in each AR case, and that the values at each position for the different AR cases only vary by about one order of magnitude, in contrast to the 3 to 7 orders of magnitude variation in the vacuum cases. This means that not only do the nanorods overcome the distance dependent decay of the

RET rate (even more effectively than do nanospheres), they also have the ability to fill the "minima" (such as position ③) associated with the vacuum case.

IV. CONCLUSIONS

We have presented a general but simple computational scheme to simulate RET in inhomogeneous absorbing and dispersive media based on a real-time electrodynamics approach, termed the time-domain electrodynamics resonance energy transfer (TED-RET) method. The main result, Eq. (14),

$$M(\omega, \mathbf{r_D}, \mathbf{r_A}) = -\mu^{eg}(\mathbf{r_A})\mu^{ge}(\mathbf{r_D})\frac{\mathbf{e_A}\cdot\mathbf{E}^{\mathrm{D}}(\mathbf{r_A},\omega)}{\mathrm{p_{ex}}(\omega)},$$

can be employed to study RET in the vicinity of any type of nanostructure (not necessarily plasmonic) as long as the relative permeability is close to 1, e.g., gold, water, silver. For homogeneous media, the numerical results from the present approach are exactly the same as those from quantum electrodynamics, and are robust under different numerical settings, including the wavelength and pulse length of the source time signal generated by the donor molecule. We demonstrate the usefulness of the TED-RET approach by examining energy transfer between molecules in the presence of gold spheres and rods, and we show that enhancement factors as high as 10^6 can occur. Furthermore, the calculated transition matrix elements indicate that the nanoparticles can dramatically reduce long-range decay of the RET rate, such that the transfer rate for over hundreds of nanometers can be comparable to that over tens of nm. In addition, factors related to the relative orientations of the donor and acceptor molecules can be significantly modified, leading in some cases to reduced RET rates but in other cases to greatly enhanced rates. Note that this study does not consider the effect of a dielectric medium on the transition dipole that leads to enhancement of the dipole by a local field factor $[(\epsilon_r+2)/3]^2$.[55,93] This extra factor, which arises in the quantum electrodynamic description of energy transfer[55] when the dielectric medium is in direct contact with the dipole, is important for the homogeneous medium example that we considered, but is not relevant for dipoles in vacuum that are several nm from gold nanostructures. Indeed, our approach does correctly incorporates local field effects associated with nanostructures that are not in direct contact with the donor and acceptor. Finally, we believe that these results demonstrate that plasmonic nanoparticles provide exciting opportunities for RET applications, such as in light harvesting and sensing.

ACKNOWLEDGMENTS

This research was supported in part through the computational resources and staff contributions provided for the Quest high performance computing facility at Northwestern University which is jointly supported by the Office of the Provost, the Office for Research, and Northwestern University Information Technology. This work was supported by U.S. National Science Foundation under grant number CHE-1465045.

[1] R. Jin, Y. Cao, C. A. Mirkin, K. L. Kelly, G. C. Schatz, and J. G. Zheng, Science **294**, 1901 (2001).
[2] C. L. Haynes and R. P. Van Duyne, J. Phys. Chem. B **105**, 5599 (2001).
[3] M. A. El-Sayed, Acc. Chem. Res. **37**, 326 (2004).
[4] A. Courty, A. I. Henry, N. Goubet, and M. P. Pileni, Nat. Mater. **6**, 900 (2007).
[5] J. Park, J. Joo, S. G. Kwon, Y. Jang, and T. Hyeon, Angew. Chem. Int. Ed. **46**, 4630 (2007).
[6] M. P. Pileni, J. Phys. Chem. C **111**, 9019 (2007).
[7] A. R. Tao, S. Habas, and P. Yang, Small **4**, 310 (2008).
[8] M. Grzelczak, J. Perez-Juste, P. Mulvaney, and L. M. Liz-Marzan, Chem. Soc. Rev. **37**, 1783 (2008).
[9] J. Lee, W. Hasan, C. L. Stender, and T. W. Odom, Acc. Chem. Res. **41**, 1762 (2008).
[10] X. Lu, M. Rycenga, S. E. Skrabalak, B. Wiley, and Y. Xia, Annu. Rev. Phys. Chem. **60**, 167 (2009).
[11] J. E. Millstone, S. J. Hurst, G. S. Métraux, J. I. Cutler, and C. A. Mirkin, Small **5**, 646 (2009).
[12] C. Burda, X. Chen, R. Narayanan, and M. A. El-Sayed, Chem. Rev. **105**, 1025 (2005).
[13] B. Wiley, Y. Sun, and Y. Xia, Acc. Chem. Res. **40**, 1067 (2007).
[14] D. V. Talapin, J.-S. Lee, M. V. Kovalenko, and E. V. Shevchenko, Chem. Rev. **110**, 389 (2010).
[15] K. L. Kelly, E. Coronado, L. L. Zhao, and G. C. Schatz, J. Phys. Chem. B **107**, 668 (2003).
[16] C. J. Murphy, T. K. Sau, A. M. Gole, C. J. Orendorff, J. Gao, L. Gou, S. E. Hunyadi, and T. Li, J. Phys. Chem. B **109**, 13857 (2005).
[17] P. K. Jain, X. Huang, I. H. El-Sayed, and M. A. El-Sayed, Acc. Chem. Res. **41**, 1578 (2008).
[18] M. P. Pileni, Acc. Chem. Res. **41**, 1799 (2008).
[19] A.-I. Henry, J. M. Bingham, E. Ringe, L. D. Marks, G. C. Schatz, and R. P. Van Duyne, J. Phys. Chem. C **115**, 9291 (2011).
[20] S. Lal, N. K. Grady, J. Kundu, C. S. Levin, J. B. Lassiter, and N. J. Halas, Chem. Soc. Rev. **37**, 898 (2008).
[21] M. Hu, J. Chen, Z.-Y. Li, L. Au, G. V. Hartland, X. Li, M. Marquez, and Y. Xia, Chem. Soc. Rev. **35**, 1084 (2006).
[22] K. A. Willets and R. P. V. Duyne, Annu. Rev. Phys. Chem. **58**, 267 (2007).
[23] K. M. Mayer and J. H. Hafner, Chem. Rev. **111**, 3828 (2011).
[24] K. Saha, S. S. Agasti, C. Kim, X. Li, and V. M. Rotello, Chem. Rev. **112**, 2739 (2012).
[25] M. Li, S. K. Cushing, and N. Wu, Analyst **140**, 386 (2015).
[26] S. Eustis and M. A. El-Sayed, Chem. Soc. Rev. **35**, 209 (2006).
[27] T. Förster, Ann. Phys. **437**, 55 (1948).
[28] R. Roy, S. Hohng, and T. Ha, Nat. Meth. **5**, 507 (2008).
[29] B. E. Hardin, E. T. Hoke, P. B. Armstrong, J.-H. Yum, P. Comte, T. Torres, J. M. J. Fréchet, M. K. Nazeeruddin, M. Grätzel, and M. D. McGehee, Nat. Photon. **3**, 406 (2009).
[30] V. Sundström, T. Pullerits, and R. van Grondelle, J. Phys. Chem. B **103**, 2327 (1999).
[31] T. Renger, V. May, and O. Kühn, Phys. Rep. **343**, 137 (2001).
[32] X. Hu, T. Ritz, A. Damjanovic, F. Autenrieth, and K. Schulten, Q. Rev. Biophys. **35**, 1 (2002).

[33] M. A. Baldo, M. E. Thompson, and S. R. Forrest, Nature **403**, 750 (2000).

[34] I. L. Medintz, A. R. Clapp, H. Mattoussi, E. R. Goldman, B. Fisher, and J. M. Mauro, Nat. Mater. **2**, 630 (2003).

[35] L. Stryer and R. P. Haugland, Proc. Natl. Acad. Sci. USA **58**, 719 (1967).

[36] C. G. dos Remedios and P. D. J. Moens, J. Struct. Biol. **115**, 175 (1995).

[37] A. A. Deniz, M. Dahan, J. R. Grunwell, T. Ha, A. E. Faulhaber, D. S. Chemla, S. Weiss, and P. G. Schultz, Proc. Natl. Acad. Sci. U.S.A. **96**, 3670 (1999).

[38] S. Weiss, Nat. Struct. Mol. Biol. **7**, 724 (2000).

[39] B. Schuler, E. A. Lipman, and W. A. Eaton, Nature **419**, 743 (2002).

[40] B. Schuler and W. A. Eaton, Curr. Opin. Struct. Biol. **18**, 16 (2008), folding and Binding / Protein-nucleic acid interactions.

[41] G. P. Acuna, M. Bucher, I. H. Stein, C. Steinhauer, A. Kuzyk, P. Holzmeister, R. Schreiber, A. Moroz, F. D. Stefani, T. Liedl, F. C. Simmel, and P. Tinnefeld, ACS Nano **6**, 3189 (2012).

[42] X. Zhang, C. A. Marocico, M. Lunz, V. A. Gerard, Y. K. Gun'??ko, V. Lesnyak, N. Gaponik, A. S. Susha, A. L. Rogach, and A. L. Bradley, ACS Nano **8**, 1273 (2014).

[43] S. Khatua, P. M. R. Paulo, H. Yuan, A. Gupta, P. Zijlstra, and M. Orrit, ACS Nano **8**, 4440 (2014).

[44] J. Li, S. K. Cushing, F. Meng, T. R. Senty, A. D. Bristow, and N. Wu, Nat. Photon. **9**, 601 (2015).

[45] J. de Torres, P. Ferrand, G. Colas des Francs, and J. Wenger, ACS Nano **10**, 3968 (2016).

[46] J. de Torres, M. Mivelle, S. B. Moparthi, H. Rigneault, N. F. Van Hulst, M. F. García-Parajó, E. Margeat, and J. Wenger, Nano Lett. **16**, 6222 (2016).

[47] C. Sönnichsen, B. M. Reinhard, J. Liphardt, and A. P. Alivisatos, Nat. Biotech. **23**, 741 (2005).

[48] G. Li, C. Cherqui, N. W. Bigelow, G. Duscher, P. J. Straney, J. E. Millstone, D. J. Masiello, and J. P. Camden, Nano Lett. **15**, 3465 (2015).

[49] T. Förster, Discuss. Faraday Soc. **27**, 7 (1959).

[50] T. Förster, Radiat. Res. Suppl. **2**, 326 (1960).

[51] D. L. Andrews, in Tutorials in Complex Photonic Media, edited by M. A. Noginov, M. W. McCall, G. Dewar, and N. I. Zheludev (SPIE Press, Bellingham, WA, 2009) pp. 439–478.

[52] M. J. Stephen, J. Chem. Phys. **40**, 669 (1964).

[53] E. A. Power and T. Thirunamachandran, Phys. Rev. A **28**, 2671 (1983).

[54] D. L. Andrews and B. S. Sherborne, J. Chem. Phys. **86**, 4011 (1987).

[55] G. Juzeliūnas and D. L. Andrews, Phys. Rev. B **49**, 8751 (1994).

[56] G. Juzeliūnas and D. L. Andrews, "Quantum electrodynamics of resonance energy transfer," in Advances in Chemical Physics (John Wiley & Sons, Inc., 2000) pp. 357–410.

[57] G. J. Daniels, R. D. Jenkins, D. S. Bradshaw, and D. L. Andrews, J. Chem. Phys. **119**, 2264 (2003).

[58] G. D. Scholes, Annu. Rev. Phys. Chem. **54**, 57 (2003).

[59] C. Curutchet and B. Mennucci, J. Am. Chem. Soc. **127**, 16733 (2005).

[60] C. Curutchet, J. Kongsted, A. Muñoz Losa, H. Hossein-Nejad, G. D. Scholes, and B. Mennucci, J. Am. Chem. Soc. **133**, 3078 (2011).

[61] J. D. Dow, Phys. Rev. **174**, 962 (1968).

[62] G. Juzeliūnas and D. L. Andrews, Phys. Rev. B **50**, 13371 (1994).

[63] G. Juzeliūnas, Phys. Rev. A **53**, 3543 (1996).

[64] H. T. Dung, L. Knöll, and D.-G. Welsch, Phys. Rev. A **65**, 043813 (2002).

[65] H. Morawitz, Phys. Rev. **187**, 1792 (1969).

[66] K. Drexhage, J. Lumin. **1**, 693 (1970).

[67] R. Matloob, Phys. Rev. A **62**, 022113 (2000).

[68] F. Le Kien and K. Hakuta, Phys. Rev. A **75**, 013423 (2007).

[69] A. Moroz, Opt. Commun. **283**, 2277 (2010).

[70] A. Poudel, X. Chen, and M. A. Ratner, J. Phys. Chem. Lett. **7**, 955 (2016).

[71] P. Stehle, Phys. Rev. A **2**, 102 (1970).

[72] P. Milonni and P. Knight, Opt. Commun. **9**, 119 (1973).

[73] M. R. Philpott, Chem. Phys. Lett. **19**, 435 (1973).

[74] H. Rigneault and S. Monneret, Phys. Rev. A **54**, 2356 (1996).

[75] D. T. Alves, C. Farina, and A. C. Tort, Phys. Rev. A **61**, 034102 (2000).

[76] R. El-Ganainy and S. John, New J. Phys. **15**, 083033 (2013).

[77] H. Chew, Phys. Rev. A **38**, 3410 (1988).

[78] H. T. Dung, L. Knöll, and D.-G. Welsch, Phys. Rev. A **62**, 053804 (2000).

[79] C. E. Reed, J. Giergiel, J. C. Hemminger, and S. Ushioda, Phys. Rev. B **36**, 4990 (1987).

[80] H. Chew, J. Chem. Phys. **87**, 1355 (1987).

[81] H. T. Dung, L. Knöll, and D.-G. Welsch, Phys. Rev. A **64**, 013804 (2001).

[82] W. Żakowicz and M. Janowicz, Phys. Rev. A **62**, 013820 (2000).

[83] T. Søndergaard and B. Tromborg, Phys. Rev. A **64**, 033812 (2001).

[84] V. V. Klimov and M. Ducloy, Phys. Rev. A **69**, 013812 (2004).

[85] D. P. Fussell, R. C. McPhedran, and C. Martijn de Sterke, Phys. Rev. A **71**, 013815 (2005).

[86] C. A. Marocico and J. Knoester, Phys. Rev. A **79**, 053816 (2009).

[87] L. A. Blanco and F. J. García de Abajo, Phys. Rev. B **69**, 205414 (2004).

[88] J. P. Dowling and C. M. Bowden, Phys. Rev. A **46**, 612 (1992).

[89] K. Busch, N. Vats, S. John, and B. C. Sanders, Phys. Rev. E **62**, 4251 (2000).

[90] Y. Yang and S.-Y. Zhu, Phys. Rev. A **62**, 013805 (2000).

[91] D. P. Fussell, R. C. McPhedran, and C. Martijn de Sterke, Phys. Rev. E **70**, 066608 (2004).

[92] D. P. Fussell, R. C. McPhedran, and C. Martijn de Sterke, Phys. Rev. E **72**, 046605 (2005).

[93] G. D. Scholes and G. R. Fleming, J. Phys. Chem. B **104**, 1854 (2000).

[94] M. Valiev, E. J. Bylaska, N. Govind, K. Kowalski, T. P. Straatsma, H. J. J. V. Dam, D. Wang, J. Nieplocha, E. Apra, T. L. Windus, and W. A. d. Jong, Comp. Phys. Comm. **181**, 1477 (2010).

[95] C. Adamo and V. Barone, J. Chem. Phys. **110**, 6158 (1999).

[96] T. H. Dunning, J. Chem. Phys. **90**, 1007 (1989).

[97] Lumerical Solutions, Inc. http://www.lumerical.com/tcad-products/fdtd/.

[98] P. B. Johnson and R. W. Christy, Phys. Rev. B **6**, 4370 (1972).

[99] F. C. Spano and C. Silva, Annu. Rev. Phys. Chem. **65**, 477 (2014).

[100] M. J. Banholzer, S. Li, J. B. Ketter, D. I. Rozkiewicz, G. C. Schatz, and C. A. Mirkin, J. Phys. Chem. C **112**, 15729 (2008).